Supporting Information

Directional and Rotational Motions of Nanoparticles on Plasma Membranes as Local Probes of Surface Tension Propagation

Shixin Li,[†] Zengshuai Yan,[‡] Zhen Luo,[‡] Yan Xu,[‡] Fang Huang,[†] Guoqing Hu,[*,‖,§] Xianren Zhang,[⊥] and Tongtao Yue[*,†,‡]

[†]State Key Laboratory of Heavy Oil Processing, China University of Petroleum (East China), Qingdao 266580, China

[‡]Center for Bioengineering and Biotechnology, College of Chemical Engineering, China University of Petroleum (East China), Qingdao 266580, China

[‖]State Key Laboratory of Nonlinear Mechanics (LNM), Institute of Mechanics, Chinese Academy of Science, Beijing 100190, China

[§]School of Engineering Science, University of Chinese Academy of Sciences, Beijing 100049, China

[⊥] State Key Laboratory of Organic-Inorganic Composites, Beijing University of Chemical Technology, Beijing 100029, China

Table S1 The interaction parameters between two types of beads in the simulations.

	Head (H)	Tail (T)	NP (P)	Ligand (L)	Water (W)
Head (H)	25	50	25	0-15	25
Tail (T)	50	15	80	80	80
NP (P)	25	80	50	50	50
Ligand (L)	0-15	80	50	50	50
Water (W)	25	80	50	50	25

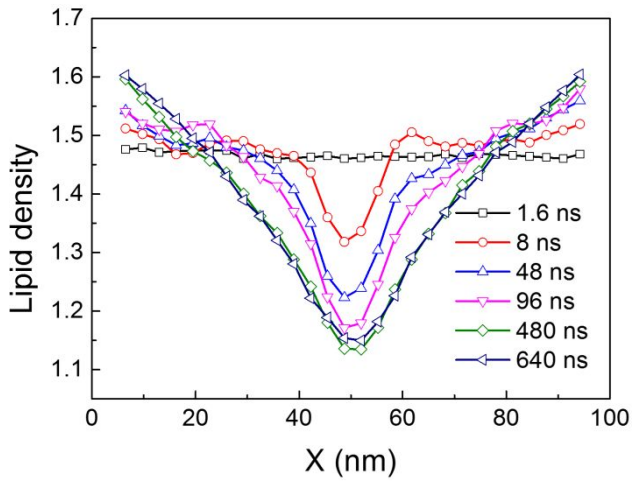

Figure S1. Distributions of the lipid density along x direction at different time points showing the system reaching the dynamic equilibrium state via tension propagation.

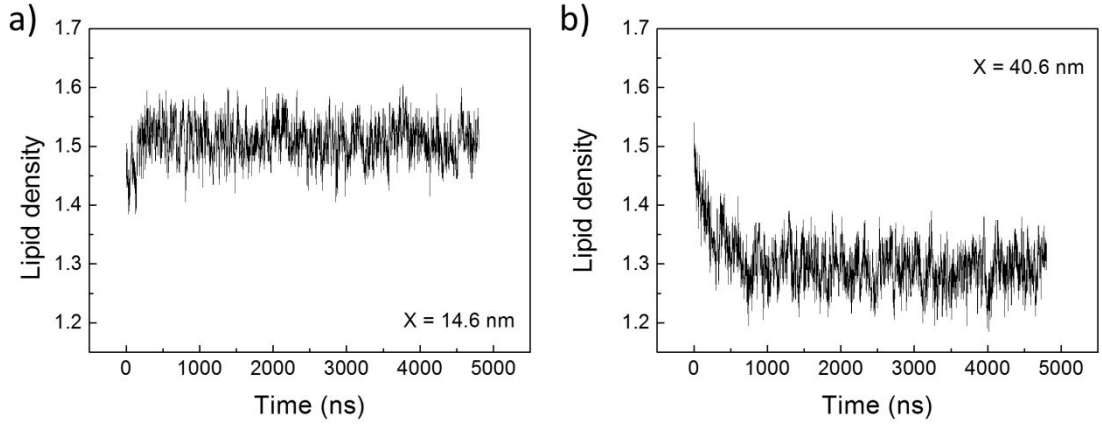

Figure S2. Time evolutions of the local lipid density at two different positions along x direction. The tension gradient was controlled by setting ρ_{LNPA}^{low} = 1.1 and ρ_{LNPA}^{high} = 1.6.

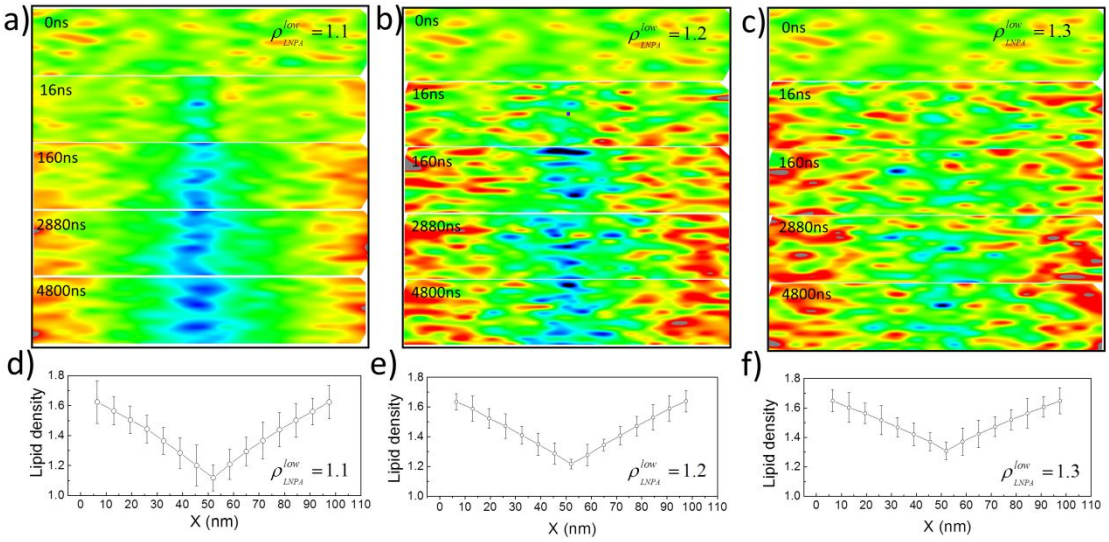

Figure S3. Effect of the defined tension gradient on the tension propagation. (a-c) Time sequences of the lipid density distribution. (d-f) The final distributions of lipid density along x direction. The local lipid density at the terminal region was fixed at ρ_{LNPA}^{high} = 1.6, with that at the central region being varied from ρ_{LNPA}^{low} = 1.1 (a, d) to 1.2 (b, e) and 1.3 (c, f).

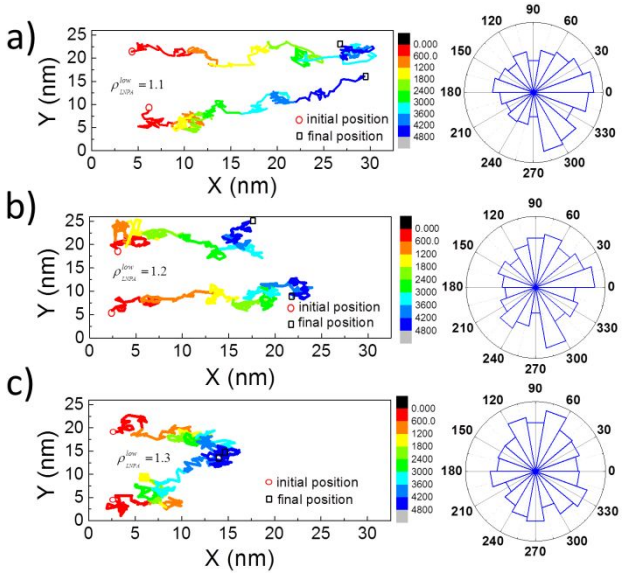

Figure S4. Diffusion trajectories of two lipid molecules in membranes under different tension gradients. (a) ρ_{LNPA}^{low} = 1.1 and ρ_{LNPA}^{high} = 1.6. (b) ρ_{LNPA}^{low} = 1.2 and ρ_{LNPA}^{high} = 1.6. (c) ρ_{LNPA}^{low} = 1.3 and ρ_{LNPA}^{high} = 1.6. The right panel shows the calculated average distribution of the turning angle.

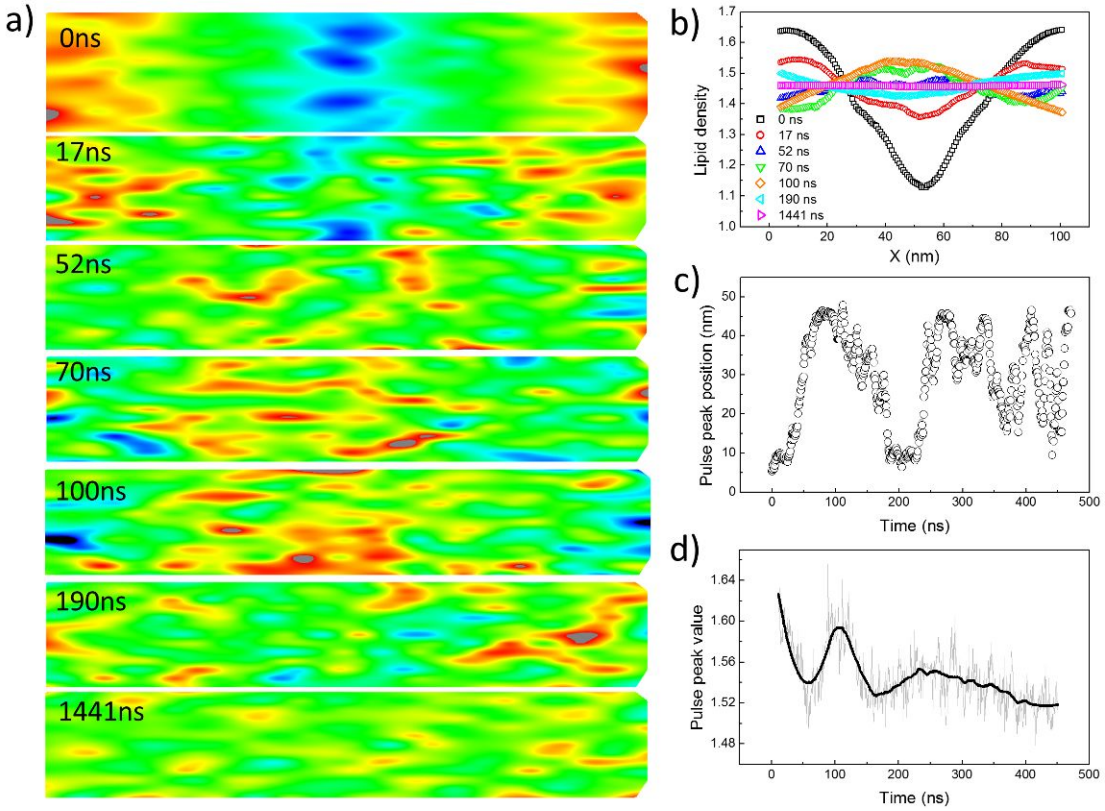

Figure S5. Propagation of two lipid density pulses activated from the terminal regions by shutting off the addition and deletion moves of lipids. a) Time sequence of the lipid density distribution along the membrane. b) Distributions of the average lipid density along x direction at different time points. c) Time evolution of the pulse position activated from the left terminal region. d) Time evolution of the pulse strength. The initial structure was obtained from the final structure shown in Figure 1c.

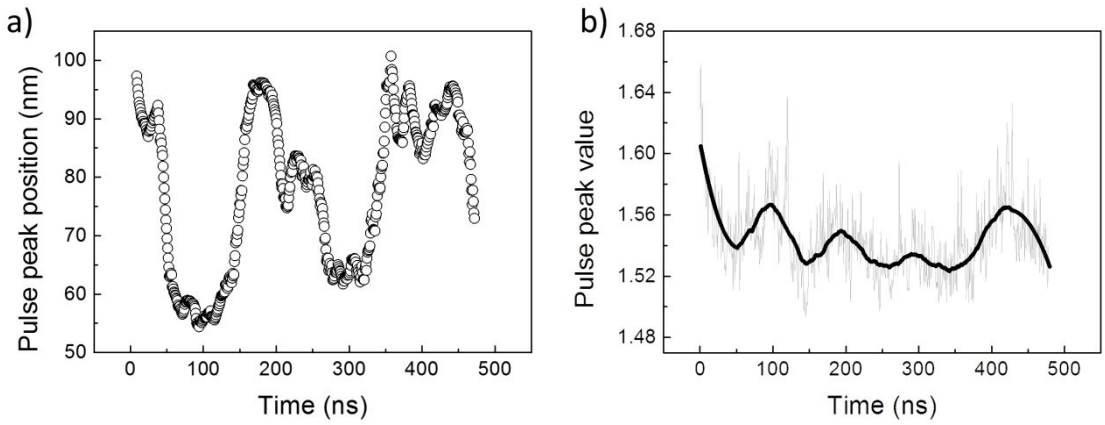

Figure S6. Evolution of the lipid density pulse activated from the right terminal region. (a) Time evolution of the pulse peak position along x direction. (b) Time evolution of the pulse peak value.

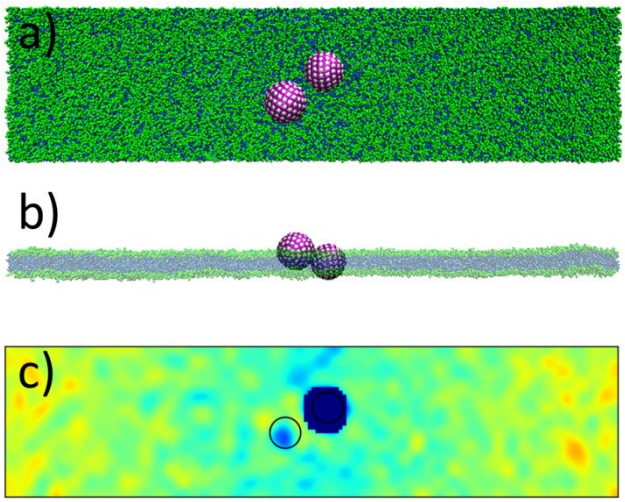

Figure S7. The final structure of two NPs gathering at the membrane center from both the top (a) and side (b) views, from which one NP was found to be anchored into the membrane interior. c) The final distribution of the lipid density.

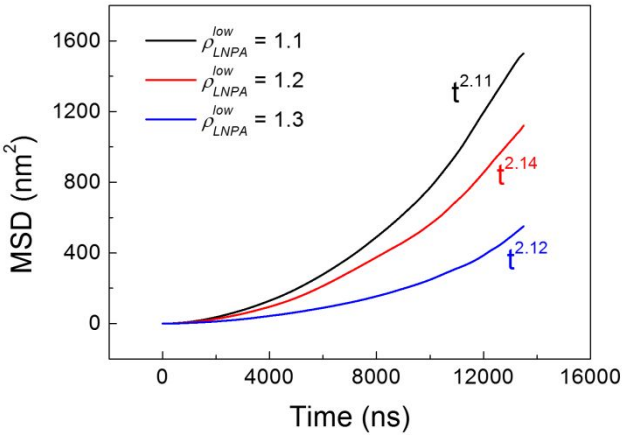

Figure S8. Mean-square displacement (MSD) for NPs moving on the plasma membrane of three gradients of surface tension.

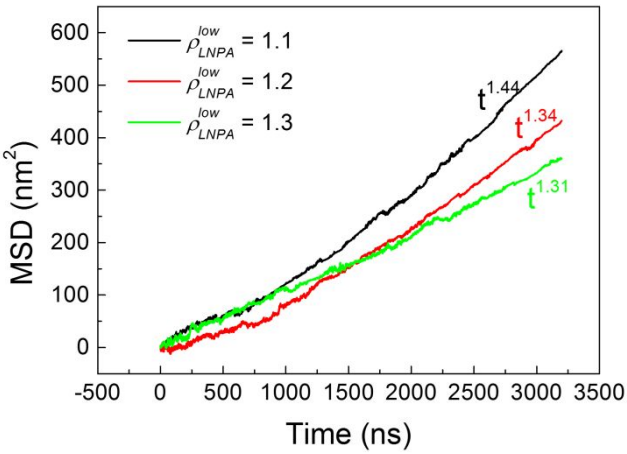

Figure S9. Mean-square displacement (MSD) of lipids under different tension gradient.

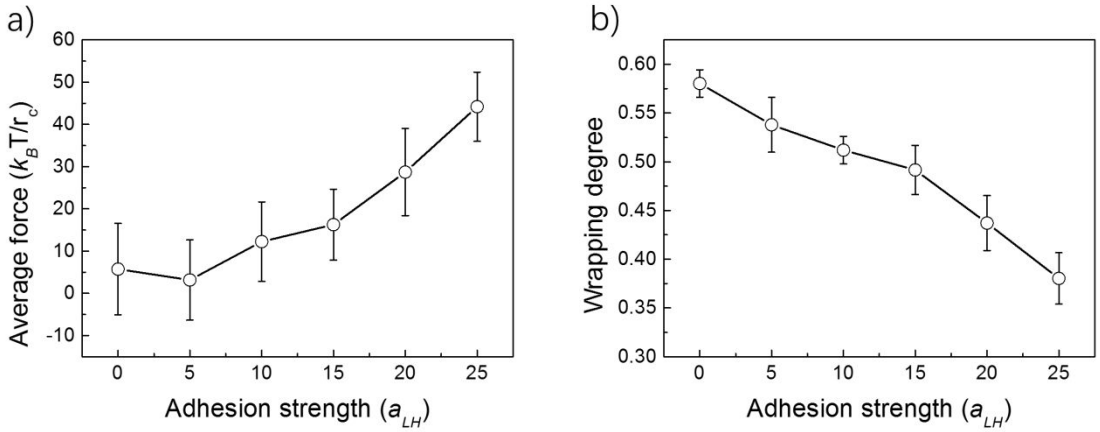

Figure S10. The effect of NP-membrane adhesion strength (a_{LH}) on the average force exerted by flowing lipids on NPs (a) and the steady membrane wrapping degree (b).

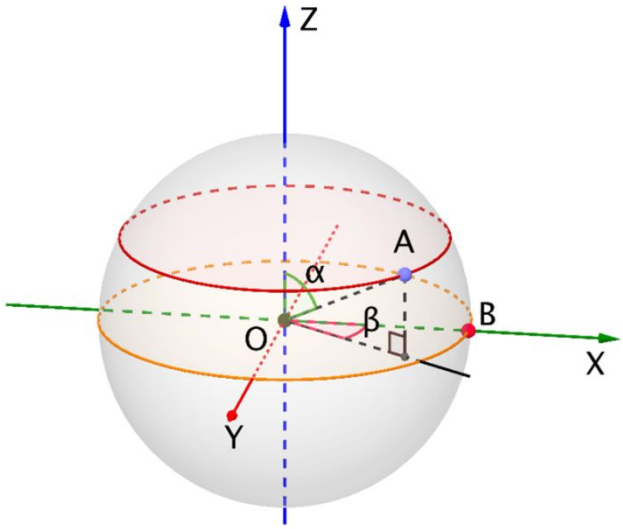

Figure S11. Definition of both the rolling angle (α) and the tilt angle (β) of the NP.

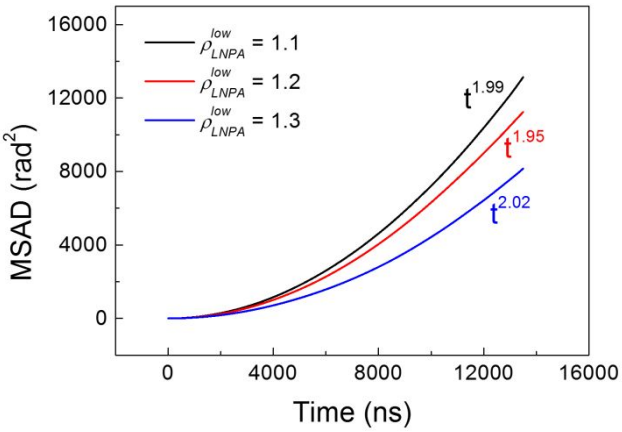

Figure S12. Mean square angular displacement (MSAD) of NPs rotating on the membrane with three gradients of surface tension.

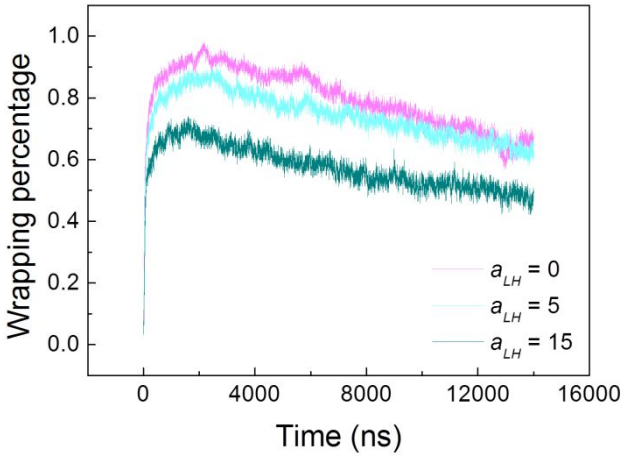

Figure S13. Time evolutions of the wrapping percentage of NPs by the membrane under different membrane adhesion strengths. The tension gradient was controlled by setting ρ_{LNPA}^{low} = 1.1 and ρ_{LNPA}^{high} = 1.6.